DOI 10.4430/bgta0342

The uncertainty analysis of seismic reflection coefficient estimation based on polynomial chaos expansion

M.R. Qaderi[1], M.A. Riahi[2] and R. Nikrouz[1]

[1] *Geology Group, University of Urmia, Iran*
[2] *Institute of Geophysics, University of Tehran, Iran*

(Received: 15 September 2019; accepted: 19 August 2020)

ABSTRACT To estimate the seismic reflection coefficients, using deterministic computational methods, the velocities and density of a layer are assumed to be constant; this assumption is not required when using statistical analysis, such as the polynomial chaos expansion. If we let the input parameters of a layer to vary, the determination of the reflection coefficient will have uncertainty. Accurate determination of the reflection coefficient is valuable for the correct modelling of wave propagation amplitude. The standard deviation is an indicator of our data distribution. To reduce the uncertainty of the reflection coefficient estimated using the Zoeppritz equations, standard deviations are considered for the input parameters. In this paper, the following steps are taken to investigate the changes of the reflection coefficient curve of layer with depth: 1) the P-, and S-wave velocities, and density, are used in the Zoeppritz equations to determine the reflection coefficients in the polynomial chaos expansion; 2) the accuracy of the estimated reflection coefficients is better, while the standard deviations for the input parameters is low. Using the lower standard deviations for the input parameters resulted highly accurate in estimating reflection coefficients and critical angle.

Key words: seismic parameter, reflection coefficient curve, standard deviation, Poisson's ratio, uncertainty.

1. Introduction

The Poisson's ratio is a measure of Poisson's effect, a phenomenon in which material tends to expand perpendicular to the compression direction. Likewise, if the material is stretched rather than compressed, it will shrink in a direction perpendicular to the stretch. Like many other materials, rocks exhibit Poisson's effect when exposed to stress. Excessive erosion and sedimentation of the Earth's crust can cause, or decrease, a great deal of vertical stress on the underlying rocks. This causes the rock to expand or shrink in the vertical direction and, also, to deform due to the Poissons effect. Poisson's ratio is one of the most important physical properties of rocks that will allow us to gain a better understanding of the mechanical behaviour of subsurface layers (Beer, 2014).

The Zoeppritz (1919) equations specify the reflection and transmission of the wave propagation coefficients as a function of the incidence angle. Still, these equations do not accurately represent how the amplitude changes with changing the physical properties of the rock. The approximations of the Zoepprites equations are simpler and more general than the general equations. Among the well known approximations presented for the Zoeppritz equation, those suggested by Aki

and Richards (1980), Shuey (1985), Mallick and Frazer (1991), Fatti *et al*. (1994), Verm and Hilterman (1995), Afzal *et al*. (2018), and Zhang *et al*. (2018) are worth citing. Beforehand, based on these approximations, reflection/transmission coefficients and different seismic attributes have been extracted.

The Polynomial Chaos Expansion (PCE) takes each complex function as an input and, by the coefficients contained within the polynomial, as well as the polynomial variables, it becomes a function with simplified polynomials (Chaitanya, 2017). In this paper, we derive the nonlinear equations of Zoeppritz (1919) with the PCE in the form of a univariate finite exponent and easily calculate the uncertainty of the reflection coefficient of the PCE in the form of a univariate finite exponent.

Based on the Huygens theorem, the wave propagation velocity in homogeneous environments is constant. The propagation velocity of seismic waves in an elastic environment depends on reflection coefficients and the density of the medium.

Generally, the factors affecting the wave velocity can be divided into two categories: the first is related to the inherent physical and lithological properties of the rock, such as porosity, of the pore types, composition, grain size, texture, and the rock fabric. The second category is related to the environmental characteristics of the medium, such as burial depth, confining pressure, and the age of the sediments. In real geological environments, the wave propagation velocity is affected by a combination of these factors.

Each factor is investigated independently (Kearey *et al*., 2002):

- depth: the wave velocity increases with increasing depth;
- compaction: the wave velocity increases with increasing compaction;
- density: the wave velocity increases with increasing the density of the medium;
- confining pressure: the wave velocity increases with increasing confining pressure; this is a result of the reduction of porosity and improvement of grain contact. The effect of pressure changes on rock samples with low velocity is more than rocks with high velocity. The highest increment in confining pressures below 100 MPa is mostly related to fracture closure. In confining pressures greater than 100 MPa, as the fractures are already closed, the velocity reaches approximately a constant limit;
- porosity: it decreases the velocity as it increases (Barton, 2007).

Accordingly, the determination of wave propagation velocity in the Earth layers has an inherent uncertainty: the velocity and density uncertainties affect the reliability of estimated reflection coefficients of the media.

2. Geological setting

In this research, we used data from Borehole MI70 in the Mansouri oil field wells. The Mansouri oil field is located 100 km north of the Persian Gulf and 50 km SE of Ahwaz city. This study area is situated in the Dezful embayment that contains the Iranian oilfields, located SW of Zagros. In terms of geology, this oil field is located in the area of the Dezful embayment, NW of the Ahvaz oil field and the NE of the Shadegan oil field.

The Mansouri oilfield is located to the south of the Dezful embayment region, with the same structural trend as the Zagros fold-thrust belt. The Mansouri anticline is NW-SE elongated

and has a 30-km length and a 3.5-km width on the Asmari horizon. The Asmari Formation, of Oligo-Miocene age, is the most important reservoir in hydrocarbon fields in Iran; it is composed mainly of carbonate rocks and is steeply sloping on the deep sediments of the formation. The lower boundary of the Asmari Formation is overlain by the Pabdeh Formation. The Gachsaran Formation is the underlying upper boundary of the Asmari Formation (Motiei, 1993).

3. Data and processing procedures

The data used in this study are density and sonic logs acquired from the Borehole MI70 (Fig. 1).

To preserve signal-quality before and after these processing steps, we decompose the raw data into several time-series called Intrinsic Mode Functions (IMFs) ranging from the shortest wavelength dominated to the longest wavelength dominated subset. This procedure is the Empirical Mode Decomposition (EMD) (Flandrin, 2004).

The values of the parameters in the Borehole MI70 are as follows:

- P-wave velocity V_P = 3500-4750 m/s;
- S-wave velocity V_S = 1800-2300 m/s;
- density ρ = 2350-2550 kg/m^3.

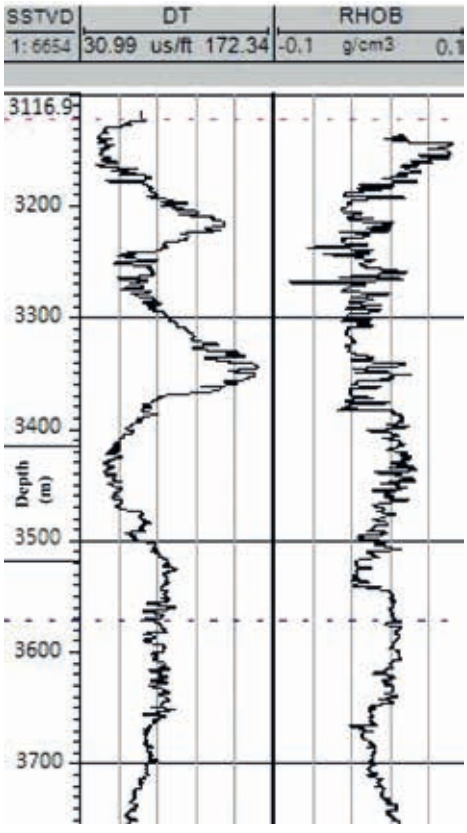

Fig. 1 - Borehole MI70 sonic and density logs.

4. Methodology

To calculate the reflection coefficient between the two layers model, one requires P-wave velocity, S-wave velocity, and density values of the two layers (Fig. 2). In this figure α and β denotes P- and S-wave average velocities of the two layers, respectively, ρ is the average density of the two layers, and θ is the average of the incident and transmitted angle.

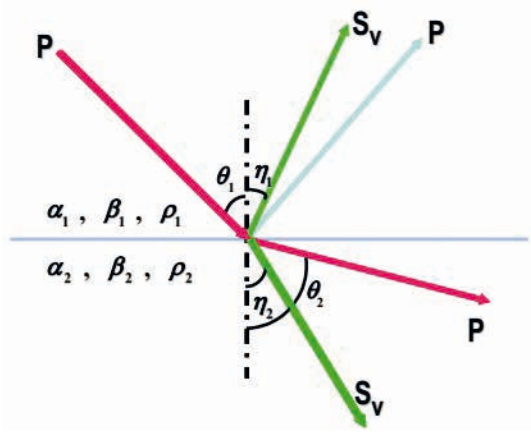

Fig. 2 - Reflected and refracted P- and S-wave rays generated by an incident P-wave ray on an interface with acoustic impedance contrast.

The following equation is conventionally used to calculate the reflection coefficient [R_{pp} (θ)] (Zong *et al.*, 2012):

$$R_{pp}(\theta) = \frac{1}{2}\left(1 - 4\left(\frac{\beta}{\alpha}\right)^2 \sin^2\theta\right)\frac{\Delta\rho}{\rho} + \frac{1}{2}(1+\tan^2\theta)\frac{\Delta\alpha}{\alpha} - 4\left(\frac{\beta}{\alpha}\right)^2 \sin^2\theta\frac{\Delta\beta}{\beta}$$

$$\alpha = (\alpha_1+\alpha_2)/2 \qquad \beta = (\beta_1+\beta_2)/2 \qquad \rho = (\rho_1+\rho_2)/2$$

$$\Delta\alpha = (\alpha_2-\alpha_1) \qquad \Delta\beta = (\beta_2-\beta_1) \qquad \Delta\rho = (\rho_2-\rho_1) \qquad (1)$$

$$\theta = (\theta_i+\theta_t)/2 \qquad \theta_t = \sin^{-1}\left[\left(\frac{\alpha_2}{\alpha_1}\right)\sin\theta_i\right]$$

We used full set well log data from Borehole MI70 located at one of the hydrocarbon fields in south-western Iran.

To model the reflection coefficient curve in terms of angle offset and reflection coefficient curve in terms of Poisson's ratio, we inspect the values of V_P, V_S, and ρ recorded from Borehole MI70 in the Zoeppritz equations and the Poisson's ratio equation based on uncertainty analysis using PCE.

5. Polynomial Chaos Expansion

In general, in PCE, the random field $u(x;\xi)$ is divided into two certain and randomised parts. The PCE of a randomised field with degree p with n_s random variables $\xi = \{\xi_i\}_{i=1}^{n_s}$ can be written:

$$u(x,\xi) = \sum_{i=0}^{p} u_i(x)\psi_i(\xi). \qquad (2)$$

Traditionally, PCE includes a complete basis of polynomials up to a fixed total order specification, in which case the total number of terms N_t in an expansion of total order p involving n_s random variables and is given by:

$$N_t = P + 1 = \frac{(p + n_s)}{p!n_s!} . \tag{3}$$

This approach is also referred to as a "total-order expansion" (Eldred and Burkardt, 2009). In Eqs. 2 and 4, ψ_i and ψ_j are the basis functions, which are orthogonal to the probability distribution functions. In a general form, we can represent the orthogonality of multidimensional inner product as (Baudin and Martinez, 2010):

$$\langle \psi_i, \psi_j \rangle = \oint \psi_i(\xi)\psi_j(\xi) PDF(\xi) d\xi = \langle \psi_i^2 \rangle \delta_{ji} . \tag{4}$$

The standard normal probability density function is given as:

$$W(x) = \frac{1}{\sqrt{2\pi}} e^{\frac{-x^2}{2}}. \tag{5}$$

The basis functions should be selected orthogonal to the probability distribution function of the uncertain input variables, for example, Legendre and Hermite basis functions are suitable for uniform and Gaussian probability distribution functions, respectively. Table 1 shows Hermite polynomials for one-dimensional parameter up to the 4th order.

Table 1 - Hermite polynomials for a one-dimensional parameter up to the 4th order (Kuzma *et al*., 2011).

Order of polynomial	
0	$\psi_0(\xi) = 1$
1	$\psi_1(\xi) = \xi$
2	$\psi_2(\xi) = \xi^2 - 1$
3	$\psi_3(\xi) = \xi^3 - 3\xi$
4	$\psi_3(\xi) = \xi^4 - 6\xi^2 + 3$

The basis functions are known; therefore, for known u_i the PCE is known. Accordingly, the problem is reduced to determining the coefficients of the chaos polynomials. As the data in this study follows a normal distribution, we obtain the polynomial chaos coefficients (PCCs) using the Gauss-Hermite quadrature method.

$$\begin{aligned} \langle \psi_i u \rangle &= \sum_{k=0}^{p} u_k \langle \psi_i \psi_k(\xi) \rangle = u_i \langle \psi_i^2 \rangle \\ u_i &= \frac{\langle u \psi_i \rangle}{\langle \psi_i^2 \rangle} \\ u &= \sum_{k=0}^{p} u_k \psi_k(\xi) = u_0\psi_0 + u_1\psi_1 + u_2\psi_2 + u_3\psi_3 + \ldots \end{aligned} \tag{6}$$

where u is the random variable (RV) represented with 1D PCE, u_k is the deterministic PCC, ψ_k is the Hermite polynomial of order k, and ξ is the Gaussian RV.

Since the basis functions are orthonormal, it can be shown that the mean value of the variance of the response can be obtained by the following formulae:

$$\mu = \langle u(x,\xi)\rangle = u_0(x)$$
$$\sigma^2 = \langle (u - \langle u\rangle)^2\rangle = \langle \left(\sum_{k=1}^{p} u_k\psi_k(\xi)\right)^2\rangle = \langle \sum_{k=1}^{p}\sum_{j=1}^{p} u_j u_k \psi_j(\xi)\psi_k(\xi)\rangle = \sum_{k=1}^{p}\sum_{j=1}^{p} u_j u_k \langle \psi_j(\xi)\psi_k(\xi)\rangle = \sum_{k=1}^{p} u_k{}^2\langle \psi_k(\xi)^2\rangle \quad (7)$$
$$\sigma^2 = \sum_{i=1}^{p} u_i{}^2\langle \psi_i{}^2\rangle .$$

PCE (O'Hagan, 2013; Schöbi *et al.*, 2014; Spiridonakos *et al.*, 2016; Sudret *et al.*, 2017) converts every complex function to several simplified terms using coefficients. One of the features of the PCE approach is that it can handle the combined effect of many parameters in a complicated function (Hariri-Ardebili and Sudret, 2019). Therefore, because of the complex manner of many geophysical studies (e.g. velocity estimation), the PCE method can be a choice for their simplification. One can filter some coefficients in PCE and retain only polynomials that depend on particular parameters; the effect of each parameter can be separated (Kuzma *et al.*, 2011).

In this paper, for the purpose of uncertainty analysis, a two-layer model, with the arbitrary incorrect variation of the selected three parameters V_P, V_S, and ρ, was selected, then, the same two-layer model was modified with correct standard deviations for the three parameters V_P, V_S, and ρ. Then, the results were compared with each other.

For this purpose, the above mentioned two-layer model was considered with the following parameters:

- first layer: P-wave velocity 3500 m/s, S-wave velocity 1800 m/s, density 2350 kg/m^3;
- second layer: P-wave velocity 4750 m/s, S-wave velocity 2300 m/s, density 2550 kg/m^3.

The standard deviation for the uncertainty is equal to $V_P = 500$ m/s, $V_S = 500$ m/s, $\rho = 100$ kg/m^3.

These values for standard deviation are calculated and obtained using the initial seismic data that were already available to us. In this sense, for example, among all seismic data, the velocity V_P of the first layer has been selected arbitrarily according to the data range, dispersion, and standard deviation.

By placing the standard deviation of the values of all three seismic parameters (V_P, V_S, and ρ) in both layers, we will have an average reflection coefficient curve of the other 512 reflection coefficients. That is, by using statistical calculations and having the standard deviation for three parameters, namely V_P, V_S, and ρ of the two layers, the curve of the reflection coefficients can be obtained. The selection of 512 curves is completely arbitrary, and one may select any number of curves. Its criterion is the correct standard deviation, which results from PCE.

Therefore, by using 100,000 different values of the three parameters (V_P, V_S, and ρ) with respect to the standard deviation of 512 curves were obtained. For realising thousands of curves in Figs. 3 and 6, all three parameters were disturbed simultaneously and not only one while fixing the other two.

One of the main ideas in this paper is the use of initial estimates of the standard deviations and then finding the correct standard deviations to obtain accurate velocity, density, reflection

Table 2 - Physical properties of different types of formation (Stanford Rock Physics Laboratory).

Type of formation	P-wave velocity (m/s)	S-wave velocity (m/s)	Density (g/ cm³)	Density of constituent crystal (g/cm³)
Scree, vegetal soil	300-700	100-300	1.7-2.4	-
Dry sands	400-1200	100-500	1.5-1.7	2.65 quartz
Wet sands	1500-2000	400-600	1.9-2.1	2.65 quartz
Saturated shales and clays	1100-2500	200-800	2.0-2.4	-
Marls	2000-3000	750-1500	2.1-2.6	-
Saturated shales and sand section	1500-2200	500-750	2.1-2.4	-
Porous and Saturated sandstones	2000-3500	800-1800	2.1-2.4	2.65 quartz
Limestones	3500-6000	2000-3300	2.4-2.7	2.71 calcite
Chalk	2300-2600	1100-1300	1.8-3.1	2.71 calcite
Salt	4500-5500	2500-3100	2.1-2.3	2.10 halite
Anhydrite	4000-5500	2200-3100	2.9-3.0	-
Dolomite	3500-6500	1900-3600	2.5-2.9	(Ca, Mg) CO_3 2.8-2.9
Granite	4500-6000	2500-3300	2.5-2.7	-
Basalt	5000-6000	2800-3400	2.7-3.1	-
Gneiss	4400-5200	2700-3200	2.5-2.7	-
Coal	2200-2700	1000-1400	1.3-1.8	-
Water	1450-1500	-	1.0	-
Ice	3400-3800	1700-1900	0.9	-
Oil	1200-1250	-	0.6-0.9	-

coefficient and Poisson's ratio. Here, a question may arise: how is the initial standard deviation calculated? In addition, which parameters is the standard deviation calculated from?

To answer the above questions, one may consider that the input data (for example, data from Borehole MI70 in this paper) contain hundreds, and maybe more, V_P, V_S, and ρ values obtained from well logging. From these data, an initial value is obtained as the mean with its related standard deviation. This standard deviation, which corresponds to a large interval of numbers, is used as the initial standard deviation for V_P, V_S, and ρ.

To perform this approach, we first obtain the curves of the wave reflection coefficients in angular distances with respect to the initial standard deviation and, then, modify the same curves with the correct standard deviations.

To examine this idea, we select as initial standard deviation the same value of 500 m/s as the standard deviation considered in the initial mode for V_P and V_S, and of 100 kg/m^3 for ρ.

6. Discussion

Fig. 3 shows the obtained results, the blue curves show the reflection coefficient (*Rpp*) of the compressional waves (initial incident P-wave and its reflected P-wave rays) in relation to the angle offset for each wave individually. The red curve depicts the average reflection coefficient

Rpp(mean) of the blue curves relative to the angle distance. The yellow curve [*Rpp(PCE)*] indicates the reflection coefficient with the initial standard deviation using PCE. What is the correct standard deviation criterion, and how does the user understand that this standard deviation is correct? The main criterion for the correct standard deviation is, firstly, the intersection of all the curves, which should be very close to the critical angle, or the zero reflection coefficient. Secondly, the Poisson's ratio curve should have a slope of approximately zero in angle offsets (degrees) close to the critical angle of the reflection coefficients (at Borehole MI70, it is 22°). The user can test the best intersection by finding the correct standard deviation with trial and error on the value of the standard deviation.

The accuracy of the initial standard deviation curves, as shown in Fig. 3, decreases with increasing angle offsets (degrees). The overlap of the average value of the *Rpp* (red curve), namely [*Rpp(mean)*], with the yellow curve, namely [*Rpp(PCE)*], obtained from PCE, drops sharply and the two curves are separated, which indicates a decrease in accuracy.

From the yellow curve, we see that, if we assign just any arbitrary values for the standard deviations of V_P, V_S, and ρ, the resulted reflection coefficients will not be correct.

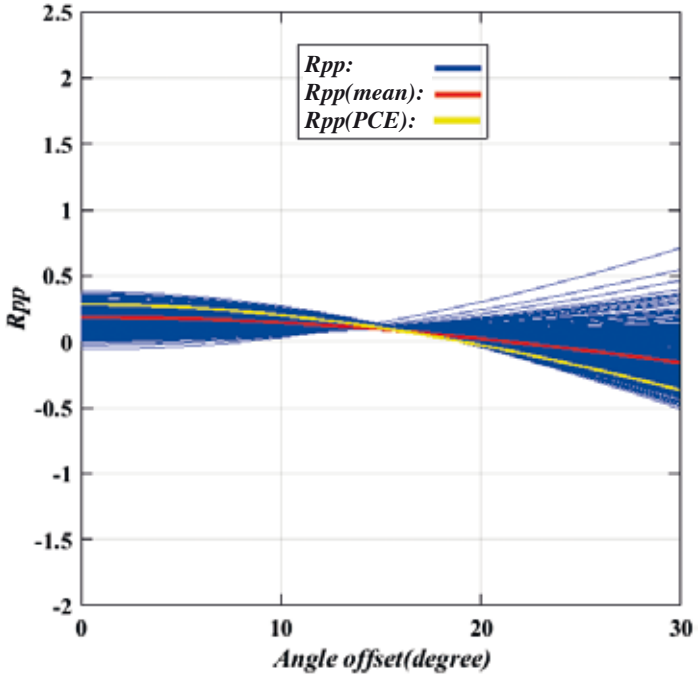

Fig. 3 - Reflection coefficient curves [*Rpp*, *Rpp(mean)*, and *Rpp(PCE)*] calculated for 0° to 30° angle offset.

In Fig. 4, the blue colour of the curve shows the reflection coefficient of the P waves (the radiation density compression wave and its reflection compression wave) versus the offset angle for each wave individually. The red curve of the reflection coefficient is the average of the blue curves compared to the angle offsets. The yellow curve shows the reflection coefficient resulting from PCE of the same waves and with the standard deviation of the angle offsets.

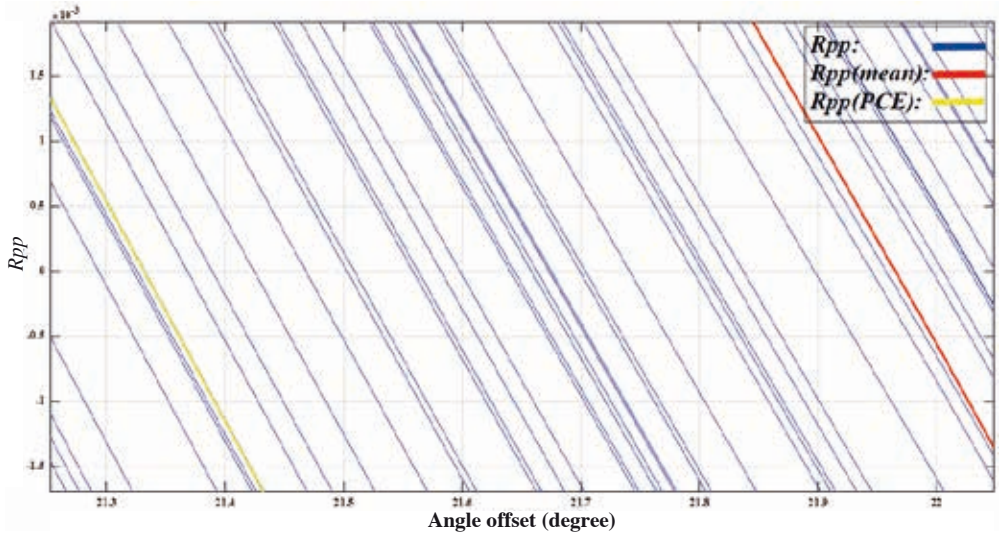

Fig. 4 - Magnification of reflection coefficient curves of *Rpp*, *Rpp(mean),* and *Rpp(PCE)* modelled in terms of 0-30° angle offsets near the critical angle.

Fig. 5 shows the obtained results for *Rpp* and *Rpp(PCE)* versus the different Poisson's ratios for 5, 22, and 30° angle offsets. As shown in Fig. 5, the initial standard deviation cannot find the Poisson's ratio with high accuracy. In this figure, the curves of the Poisson's ratio with respect to reflection coefficient, in four angle offsets (degrees), are shown, which are incorrect.

In Fig. 5, the green curve shows the average of *Rpp(mean)* of P waves (incident and reflected ray) versus the Poisson's ratio for the angular offsets of 5, 22, and 30°. The red curve shows *Rpp(PCE)* of the same P waves as the initial standard deviation versus the Poisson's ratio for the angular offsets of 5, 22, and 30°.

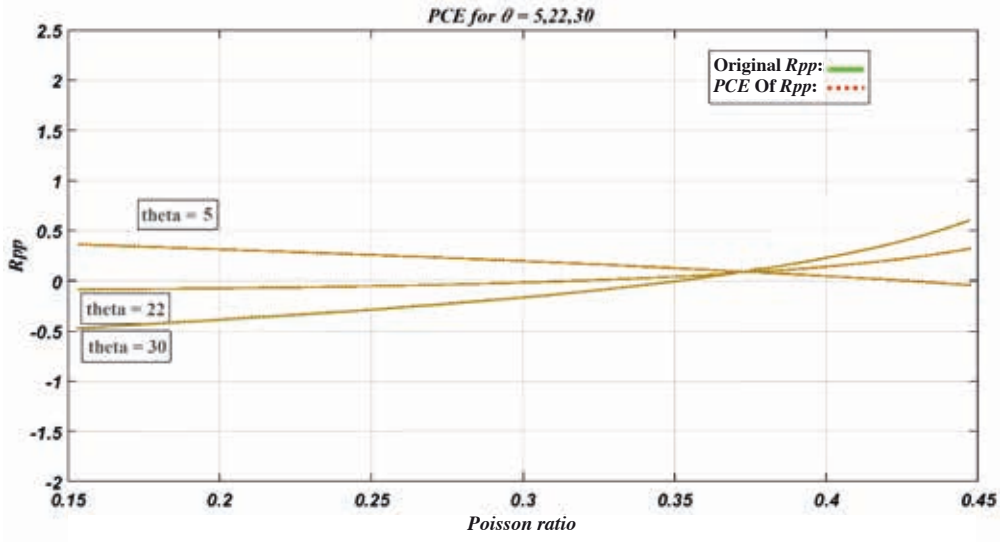

Fig. 5 - The reflection coefficient curve [*Rpp(mean)*] versus the different Poisson's ratios for 5, 22, and 30° angle offsets.

However, by performing the test and error for the standard deviation values, we will see that the standard deviation range could not be arbitrary, and many of our seismic data are invalid due to the heterogeneities of the Earth and presences of noises. Therefore, only in a specific range of standard deviation, we can carry out the best modelling of reflection coefficient relative to angle offset (Fig. 6) and relative to the Poisson's ratio (Fig. 7). The best modelling is to have the highest accuracy in the reflection coefficient curve model and, as shown in Fig. 8, having the correct standard deviation for the three parameters V_P, V_S, and ρ.

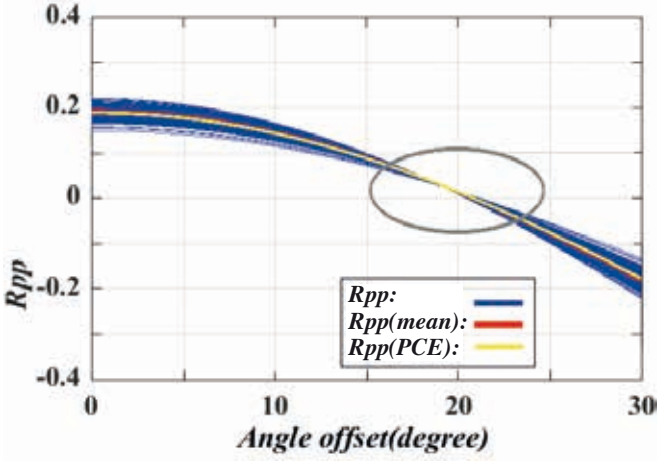

Fig. 6 - Reflection coefficient [*Rpp*, *Rpp(mean)*, and *Rpp(PCE)*] curves, modelled for 0° to 30°.

In Fig. 6, the blue colour indicates the P-wave reflection coefficients (*Rpp*) curves from the incident and reflected rays versus 0° to 30° of angle offsets. The red curve shows the average value of the blue curves of reflection coefficients versus 0° to 30° angle offsets. The yellow curve indicates reflection coefficients versus 0° to 30° angle offsets resulted from PCE with correct standard deviation. The optimum standard deviation is obtained when correct V_P, V_S, and ρ values are considered.

Fig. 7 shows that the highest accuracy the lowest uncertainty of the estimated reflection coefficient curve obtained from seismic data belongs to the velocity data obtained from the correct critical angle using PCE. We see that the least uncertainty for the reflection coefficient in critical angle offset and, according to Fig. 7, the most accurate value for the Poisson's ratio.

In Fig. 7, the green curves indicate the average value (*Rpp*) of the P-wave reflection coefficients from the incident and reflected rays for different incident angles (5, 22, and 30°) versus Poisson's ratios. Red curves indicate the reflection coefficients resulted from PCE [*Rpp(PCE)*] versus Poisson's ratios for different incident angles (5, 22, and 30°) with correct standard deviation.

At this step, one may ask: how can this method be used for real data? At what stage is its application? And what kind of problem does it solve from seismic data?

As explained above, our initial data from the Borehole MI70 include a very large range of V_P, V_S, and ρ values. For example, the initial velocity variation value in a layer may be between 3500 and 4000 m/s, which is a large range and this low accuracy is due to measurement errors, device inaccuracies, ambient noises, and Earth's heterogeneities. The user cannot, anyhow, get a unique velocity value for a single layer in a layered Earth. However, with the help of this

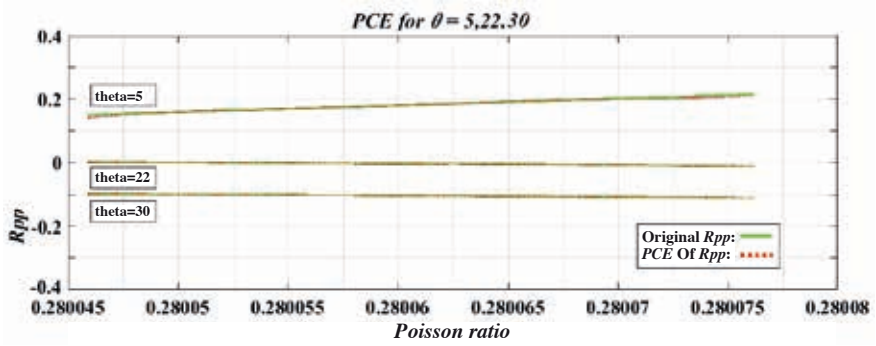

Fig. 7 - *Rpp* versus Poisson's ratios.

method, the user will be able to omit a large amount of redundant data, which are incorrect. By excluding those inaccurate data, firstly, the volume of data is reduced, the information is given more accurately, and it is presented better, in statistical terms. Secondly, by working on those data, one can determine the lithology of the layers with higher accuracy, and, thirdly, the most accurate value may be chosen for the Poisson's ratio.

At the end, we can say that this method is a sort of filtering of the raw data of V_P, V_S, and ρ values.

7. Conclusions

The data obtained from well logging contain different velocity values at different borehole depths, and some of these values are far higher or lower than their true values. This inconsistency is usually caused by the existence of drilling mud, washout, and damage zone in the borehole. Therefore, the uncertainty of well logging data can be high, and their accuracy very low.

Estimation of the reflection coefficient and Poisson's ratio, based on any interval of well logging data, using the Zoepprits equation, provides incorrect results with high uncertainty. The estimated Poisson's ratio in a layered model is obtained independent from both of the offset and angle of the incident wave. Therefore, the cross plot of Poisson's ratio at any offsets, versus the reflection coefficient, is a straight line with zero gradients at the critical angle. This study introduced that PCE is a suitable tool to estimate the reflection coefficient curve and Poisson's ratio with high accuracy and less uncertainty.

Acknowledgements. The second author would like to acknowledge the Research Council of the University of Tehran. Thanks are given to anonymous domain experts for their input and insight without which this research would not have been possible. This research did not receive any specific grant from funding agencies in the public, commercial, or not-for-profit sectors.

REFERENCES

Afzal P., Adib A. and Ebadati N.; 2018: *Delineation of seismic zonation using fractal modeling in west Yazd province, central Iran*. J. Seismol., **22**, 1377-1393, doi: 10.1007/s10950-018-9770-9.

Aki K. and Richards P.G.; 1980: *Quantitative seismology: theory and methods, 2nd ed*. Freeman W.H. and Co, San Francisco, CA, USA, 932 pp., <ISBN: 978-0716710592>.

Barton N.; 2007: *Rock quality, seismic velocity, attenuation and anisotropy*, *1st ed*. Routledge and CRS Press, Taylor and Francis Group, Abingdon on Thames, UK, 756 pp., <ISBN: 978-0415394413>.

Baudin M. and Martinez J.M.; 2010: *Polynômes de chaos sous Scilab via la librairie NISP.* In: Proc., 42èmes Journées de Statistique, Marseille, France, inria-00494680, <https://hal.inria.fr/inria-00494680>.

Beer F.; 2014: *Mechanics of materials*. McGraw-Hill Education, New York, NY, USA, 896 pp., <ISBN: 0077625234, 9780077625238>.

Chaitanya R.G.; 2017: *Uncertainty quantification in non-linear seismic wave propagation*. Master of Applied Science in Civil Engineering, Carleton University, Ottawa, ON, Canada, 172 pp., doi: 10.13140/RG.2.2.12355.40484.

Eldred M. and Burkardt J.; 2009: *Comparison of non-intrusive polynomial chaos and stochastic collocation methods for uncertainty quantification*. In: Proc., 47th AIAA Aerospace Sciences Meeting, The New Horizons Forum and Aerospace Exposition, Orlando, FL, USA, MDO-4, pp. 1-20, doi: 10.2514/6.2009-976.

Fatti J.L., Vail E.J., Smith G.C., Strauss P.J. and Levitt P.R.; 1994: *Detection of gas in sandstone reservoirs using AVO analysis: a 3-D seismic case history using the Geostack technique*. J. Geophys., **59**, 1362-1376, doi: 10.1190/1.1443695.

Flandrin P.; 2004: *Empirical mode decomposition as a filter bank*. IEEE Signal Process. Lett., **11**, 112-114, doi: 10.1109/LSP.2003.821662.

Hariri-Ardebili M.A. and Sudret B.; 2019: *Polynomial chaos expansion for uncertainty quantification of dam engineering problems*. J. Eng. Struct., **203**, 109631, doi: 10.1016/j.engstruct.2019.109631.

Kearey P., Brooks M. and Hill I.; 2002: *An introduction to geophysical exploration, 3rd ed*. Blackwell Science Publishing, Oxford, UK, 272 pp., <ISBN: 978-0-632-04929-5>.

Kuzma H.A., Zhao Y., Reagan M.T. and Rector J.M.; 2011: *Polynomial chaos for uncertainty quantification in Geophysics*. In: Expanded Abstracts, SEG Annual Meeting, San Antonio, TX, USA, pp. 2742-2746, doi: 10.1190/1.3627763.

Mallick S. and Frazer L.N.; 1991: *Reflection/transmission coefficients and azimuthal anisotropy in marine studies*. Geophys. J. Int., **105**, 241-252, doi: 10.1111/j.1365-246X.1991.tb03459.x.

Motiei H.; 1993: *Stratigraphy of Zagros*. Geological Survey of Iran Publication, Tehran, Iran, 536 pp., (in Persian).

O'Hagan A.; 2013: *Polynomial chaos: a tutorial and critique from a statistician's perspective*. School of Mathematics and Statistics, University of Sheffield, UK, 20 pp., <Corpus ID: 18348025>.

Schöbi R., Kersaudy P., Sudret B. and Wiart J.; 2014: *Combining polynomial chaos expansions and kriging*. Orange Labs Research, ETH Zurich, Switzerland, Research Report, hal-01432550, 47 pp., <https://hal.archives-ouvertes.fr/hal-01432550>.

Shuey R.T.; 1985: *A simplification of the Zoeppritz equations*. J. Geophys., **50**, 609-614, doi: 10.1190/1.1441936.

Spiridonakos M.D., Chatzi E. and Sudret B.; 2016: *Polynomial chaos expansion models for the monitoring of structures under operational variability*. ASCE-ASME J. Risk Uncertainty Eng. Syst., Part A: Civil Eng., **2**, B4016003, doi: 10.1061/AJRUA6.0000872.

Sudret B., Marelli S. and Wiart J.; 2017: *Surrogate models for uncertainty quantification: an overview*. In: Proc., 11th European Conference on Antennas and Propagation (EUCAP), pp. 793-797, doi: 10.23919/EuCAP.2017.7928679.

Verm R. and Hilterman F.; 1995: *Lithology color-coded seismic sections: the calibration of AVO cross plotting to rock properties*. The Leading Edge, **14**, 847-853, doi: 10.1190/1.1437170.

Zhang G., Hao C. and Yao C.; 2018: *Analytical study of the reflection and transmission coefficient of the submarine interface*. J. Acta Geophys., **66**, 449-460, doi: 10.1007/s11600-018-0153-y.

Zoeppritz K.; 1919: *Erdbebenwellen VIIIB*. *On the reflection and propagation of seismic waves*. Gottinger Nachrichten, I, pp. 66-84, (in German).

Zong Z.Y., Yin X.Y., Zhang F. and Wu G.C.; 2012: *Reflection coefficient equation and pre-stack seismic inversion with Young's modulus and Poisson ratio*. Chin. J. Geophys., **55**, 3786-3794, doi: 10.6038/j.issn.0001-5733.2012.11.025 (in Chinese).

Corresponding author: Mohammad Ali Riahi
Institute of Geophysics, University of Tehran
North Kargar Ave., Tehran, Iran
Phone: +98 21 61118219; e-mail: mariahi@ut.ac.ir